J Mater Sci: Mater Med (2009) 20:843–850
DOI 10.1007/s10856-008-3647-3

# Characterization of sintered titanium/hydroxyapatite biocomposite using FTIR spectroscopy

**Hezhou Ye · Xing Yang Liu · Hanping Hong**

Received: 25 February 2008 / Accepted: 3 November 2008 / Published online: 26 November 2008


**Abstract** Fourier transform infrared (FTIR) spectroscopy was employed to characterize the phase changes of hydroxyapatite ($Ca_{10}(PO_4)_6(OH)_2$, HA) in a titanium/HA biocomposite during sintering. The effects of sintering temperature and the presence of Ti on the decomposition of HA were examined. It was observed that pure HA was stable in argon atmosphere at temperatures up to 1,200°C, although the dehydroxylation of pure HA was promoted by the increase in sintering temperature. In the Ti/HA system, on the other hand, the presence of Ti accelerated dehydroxylation and the decomposition of HA was detected at a temperature as low as 800°C. Tetracalcium phosphate ($Ca_4P_2O_9$, TTCP) and calcium oxide (CaO) were the dominant products of the decomposition, but no tricalcium phosphate ($Ca_3(PO_4)_2$, TCP) was detected due to phosphorus diffusion and possible reactions during the thermal process. The main decomposed constituents of HA in Ti/HA system at high temperatures (≥1,200°C) would be CaO and amorphous phases.

## 1 Introduction

As the main mineral constituent of human bones and teeth, hydroxyapatite ($Ca_{10}(PO_4)_6(OH)_2$, HA) has attracted strong interest as a bone substitute over the past few decades. Comprehensive studies have confirmed that HA is bioactive and can stimulate new bone formation [1–4]. It has been successfully used in various implant applications [5–8]. However, the poor mechanical properties of HA as compared to nature bones, especially the low tensile strength and fracture toughness, significantly restrict its direct application as load-bearing implants, such as hip joints, tooth roots, and femur bones [9–11].

Titanium (Ti) and its alloys, on the other hand, are among the most successful metallic biomaterials for orthopaedic and dental applications due to their high specific strength, excellent corrosion resistance and good biocompatibility [12, 13]. However, Ti and Ti alloys are bioinert and can not promote tissue bonding to the implants. Further improvements in their bioactivity will greatly enhance the performance of the Ti implants. To take advantages of both the excellent biocompatibility of HA and the superior mechanical properties of titanium, a number of studies have been conducted to explore the potential of the Ti/HA composites.

Bishop proposed to produce functionally gradient materials (FGMs) by compacting Ti and HA powders [14]. The extremely high pressure used in the experiment was a challenge in practice. Furthermore, the particles were interlocked only by plastic deformation, which made the mechanical properties of the composites implausible. Chu improved the mechanical properties of the Ti/HA FGM by structural optimization and process modification. Sintering and hot isostatic pressing (HIP) were adopted in the experimental studies [15–17]. Titanium matrix biocomposites made from Ti and HA powder mixtures by powder metallurgy were reported as well [18–23]. Mechanical test confirmed that the Ti/HA composites could satisfy the requirements of some load-bearing applications. Both in vivo and in vitro studies have also illustrated the

H. Ye (✉) · H. Hong
Faculty of Engineering, University of Western Ontario,
London, Ontario N6A 5B8, Canada
e-mail: hye5@uwo.ca

X. Y. Liu
Industrial Materials Institute, National Research Council
of Canada, London, Ontario N6G 4X8, Canada

excellent biocompatibility and bioactivity of the Ti/HA composites [18–20].

Phase stability during high-temperature processing is a key concern for the fabrication of Ti/HA composites. Some previous studies have indicated that HA may decompose at relatively low temperatures with the presence of Ti. For example, Weng et al. [21] analyzed the phases in the Ti/HA composites by X-ray diffraction (XRD) after sintering the samples in the temperature range of 800°C to 930°C in vacuum. Their results showed that titanium catalyzes thermal decomposition of HA into tetracalcium phosphate ($Ca_3(PO_4)_2$, TTCP), tricalcium phosphate ($Ca_3(PO_4)_2$, TCP) and $H_2O$ when the processing temperature is higher than 800°C. Ning et al. [20, 22] characterized the phases of the Ti/HA composites with XRD after sintering at different temperatures and further observed the phases with a transmission electronic microscope. They also observed the decomposition of HA and proposed an illustrative equation for the decomposition reactions. On the other hand, Popa et al. [23] performed XRD analyses on the Ti/HA composite samples sintered at 1,160°C for 1 h in vacuum and deduced that the HA was unchanged. However, detailed and systematic investigations on the change of HA during sintering are lacking. In addition, the limited information on the phase stability of HA was obtained mainly by X-ray diffraction [20–23]. Due to the fact that many of the diffraction peaks of different calcium phosphates, such as HA, TCP, and TTCP, either overlap or locate very close to each other, it is very difficult to identify the exact phases existing in the materials by X-ray diffraction. In the case of Ti/HA composites, furthermore, a high concentration of Ti or Ti oxides will produce strong diffraction peaks that can overshadow the peaks of the calcium phosphates, which makes accurate phase identification more difficult. All these factors contribute to the divergent conclusions achieved in different studies.

Fourier transform infrared (FTIR) spectroscopy is a useful technique for rapid characterization of the chemical structures of various materials. It has been used in the study of calcium phosphates and can reveal detailed information which could not be obtained by other means [24–27]. In this study, FTIR was applied to characterizing chemical and structural changes of HA in Ti/HA composite during sintering at different temperatures.

## 2 Experimental procedures

### 2.1 Preparation of Ti/HA composite

Commercially pure (CP) titanium powder (provided by Atlantic Equipment Engineers, USA) and HA powder (provided by Pentax, Japan) were used as the starting materials. Ti/HA powder mixtures with 50 vol.% HA were sealed in glass vials under argon atmosphere and mixed in a 3D mixer (Laval Lab, Canada) for 48 h. The blended mixture were subsequently compressed uniaxially in a rigid die with an inner diameter of 12.7 mm, followed by pressureless sintering in an argon atmosphere at 800–1,200°C for 1 h. For comparison, compacts made from HA powder without Ti were also prepared and sintered under the same conditions.

### 2.2 Characterization

A FTIR spectroscopy (Mode Tensor 27, Bruker, USA) was used to investigate the chemical groups present in the samples under various processing conditions. The sintered samples were first ground into powders with a molar and pestle. Each powder sample was mixed with suitable amount of infrared grade KBr and the mixture was compressed into a thin transparent pellet using a screw-type press. The pellets were analysed in the range of 4000–400 $cm^{-1}$ at 4 $cm^{-1}$ by 128 scans. The data were collected and processed by Optical User Software (OPUS, version 5.5). For reference, pure HA samples before and after sintering were also characterized by X-ray diffraction, using a Rigaku X-ray diffractometer with Cu Kα radiation at 40 kV and 35 mA.

## 3 Results and discussion

### 3.1 Changes of pure HA during sintering

X-ray diffraction patterns of pure HA samples in the as-received condition and after sintering at different temperatures in argon are shown in Fig. 1. Up to 1,200°C, all of the patterns matched the standard JCPDS file (NO.09-0432) very well and no other peaks were detected. The sharp HA peaks indicate high degree of crystallinity of the powder. The XRD patterns evidenced that HA is thermally stable in argon atmosphere and no decomposition happened up to 1,200°C, which is consistent with the results reported by others [27, 28].

Although HA is stable in argon atmosphere in a wide temperature range, dehydroxylation can occur and results in loss of $OH^-$ groups. However, the reaction product, oxyapatite (OA) or oxyhydroxyapatite (OHA), could not be detected by XRD due to the high similarity of their crystal structures and XRD patterns to those of HA [29, 30]. In contrast, FTIR spectroscopy is an effective tool for identifying the occurrence of the dehydroxylation of HA, as shown in Fig. 2. Most of the active bands located in the range of 1,100–400 $cm^{-1}$. Some constant broad bands of low intensity appeared at 1,639, 1,994, and 2,350 $cm^{-1}$,

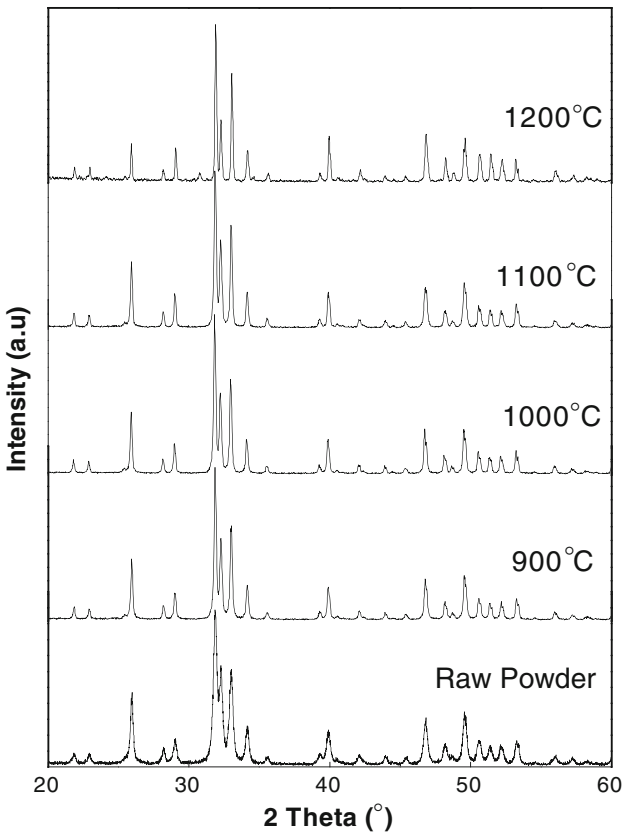


**Fig. 1** X-ray diffraction patterns for pure HA sintered in argon at various temperatures

due to the moisture and carbon dioxide present in the testing environment or absorbed during sample preparation. The broad band at 3,100–3,500 $cm^{-1}$ also corresponded to the absorbed water [31]. The weak sharp peaks at 3,571 and 632 $cm^{-1}$ were the stretching and libration bands originating from $OH^-$ in the apatite, respectively, which are the characteristic bands of HA. With the increase of the sintering temperature, the relative intensities of the $OH^-$ vibration bands decreased, indicating the occurrence and development of dehydroxylation. The peak at 632 $cm^{-1}$ changed to a shoulder in the spectrum of the HA sintered at temperatures higher than 1,000°C. The characteristic bands of $PO_4^{3-}$ groups in HA appeared at 1094 ($v_3$), 1046($v_3$), 963($v_1$), 602($v_4$), 572($v_4$), which were very stable as the temperature increased [31].

Another evidence for the dehydroxylation of HA is the appearance and intensification of new principal bands in the range of 500–400 $cm^{-1}$, which are assigned to Ca–O stretching [32, 33]. When the sintering temperature was higher than 900°C, the peak at ~435 $cm^{-1}$ and the shoulder at ~475 $cm^{-1}$ were markedly increased. In the FTIR spectrum, the absorbance intensity is proportional to the concentration of the chemical group according to Beer's Law. Therefore, the intensity ratio of the characteristic bands reflects the relative concentration of the corresponding chemical groups. Under all sintering temperatures, the ~435 $cm^{-1}$ band was stronger than the 475 $cm^{-1}$ band, indicating less than 50% dehydroxylation occurred [32]. Table 1 lists the ratio of the band intensities in the spectra of HA sintered at different temperatures. With the increase in sintering temperature, the relative intensity of hydroxyl band decreased, while that of oxyhydroxyapatite increased. Changes in the ratios also substantiated the occurrence and enhancement of dehydroxylation with increase in the sintering temperature, which can not be detected from the XRD results.

### 3.2 Changes of HA in Ti/HA composite during sintering

The FTIR spectra of the Ti/HA composite powders before and after sintering are shown in Fig. 3. The spectrum of the composite powder before sintering is identical to that of pure HA, showing all the characteristic bands at exactly the same wave numbers (Fig. 3a). In the region of 3,000–3,700 $cm^{-1}$, the broad band in all spectra is attributed to water absorption from the environment. In this region, the phosphate vibrations have no influence on the $OH^-$ mode since they are separated by the ionic bonds of the $Ca^{2+}$ [31]. As shown in the figure, the main transformation in this area is the abatement of the peak at 3,571 $cm^{-1}$ and the intensification of the peak at 3,643 $cm^{-1}$, which are due to the $OH^-$ group in HA and $Ca(OH)_2$, respectively [33, 34]. After sintering at 800°C, the two peaks at 3,571 and 3,643 $cm^{-1}$ coexist in the spectrum, indicating the HA were partially decomposed. However, because liberation band is more sensitive to temperature changes, the characteristic liberation band of $OH^-$ group of HA at 633 $cm^{-1}$ already disappeared (Fig. 3b) [27]. As the sintering temperature increased, the peak of the band of $Ca(OH)_2$ was getting stronger, while the stretching $OH^-$ band of HA vanished even after sintering at 900°C.

The bands in the region of 1,600–1,300 $cm^{-1}$ corresponds to the $v_3$ vibration mode of carbonate ions, and the peak located in 870 $cm^{-1}$ is due to the $v_2$ vibration mode of carbonate [35]. The figure clearly shows the emergence and rise of the bands due to carbonate ($CO_3^{2-}$). The carbonate group could neither be attributed to the substitution for $OH^-$ nor $PO_4^{3-}$ in the lattice of HA [34]. Both the carbonate and $Ca(OH)_2$ came from CaO, which readily integrates with atmospheric water and $CO_2$ during handling and sample preparation. To verify this point, chemically pure CaO powders were analyzed by FTIR, following the same procedure as described in the experimental section. The bands due to hydroxyl and carbonate are distinctly displayed in the spectrum (Fig. 4). Therefore, the changes in the regions of hydroxyl and carbonate bands demonstrate that HA has already started to decompose at 800°C

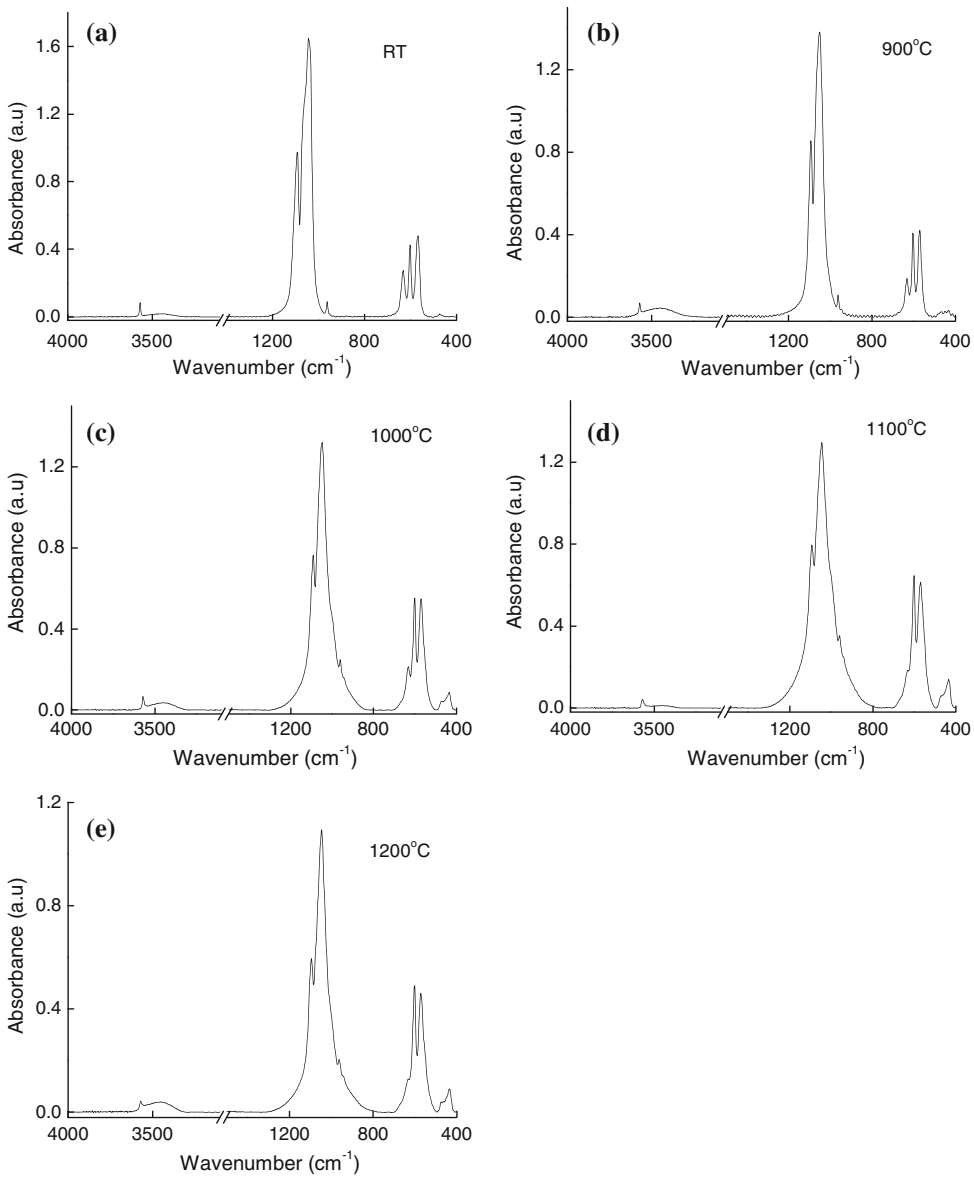


**Fig. 2** FTIR spectra of pure HA at room temperature and sintered in argon at various temperatures

**Table 1** Ratios of band intensities in the FTIR spectra of HA sintered in argon

| Sintering temperature (°C) | I(1046)/I(3571) | I(1046)/I(435) |
|---|---|---|
| RT | 19.64 | NA |
| 900 | 19.77 | NA |
| 1000 | 19.90 | 15.17939 |
| 1100 | 21.94 | 10.48033 |
| 1200 | 30.45 | 9.35223 |

and increased amount of CaO was formed in the system as sintering temperature increased.

Theoretically, there are four vibration modes present for phosphate ions, $v_1$, $v_2$, $v_3$, and $v_4$. All these modes are infrared active [31]. Table 2 shows the assignments of the peaks in the FTIR spectra. When the sintering temperature was lower than 900°C, the three different sites of $v_3$ bands at 1,093, 1,045, and 1,011 $cm^{-1}$ were observed, corresponding to the pure HA peaks in the range. Also, other characteristic peaks of HA dwell in the spectrum, implying HA was still the main phase. Besides the disappearance of the $OH^-$ liberational band at 633 $cm^{-1}$, a broad peak emerged in the 500–400 $cm^{-1}$ region. Compared with the counterparts in Fig. 2c–e, the shape of the band in Fig. 3b is significantly different. As discussed in the previous section, the new peaks in this region indicate the occurrence of dehydroxylation. Furthermore, the relative intensity between the peaks at $\sim$475 $cm^{-1}$ and that at $\sim$433 $cm^{-1}$ reflects the degree of the dehydroxylation. In Fig. 3b, the peak at 475 $cm^{-1}$ is stronger than the peak at 433 $cm^{-1}$, which means more than 50% dehydroxylation has completed [32].

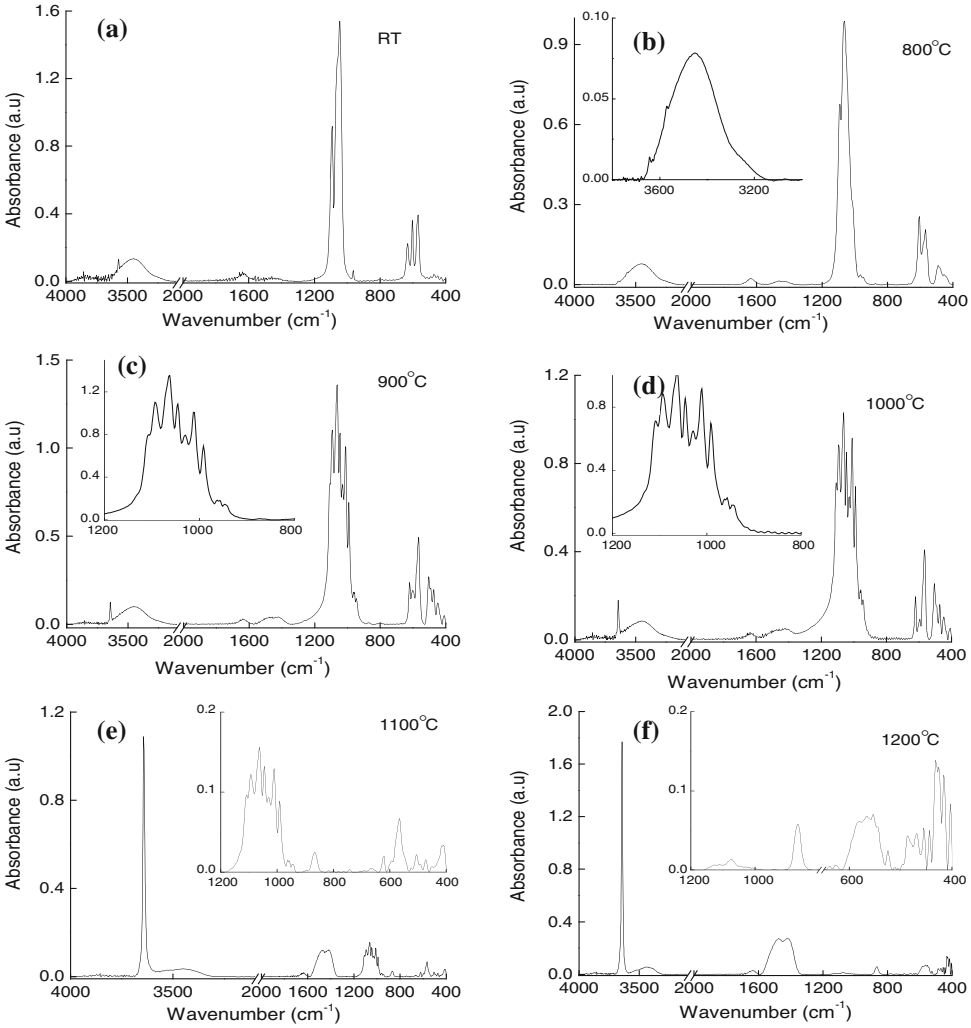


**Fig. 3** FTIR spectra of Ti/HA composite at room temperature and sintered in argon at various temperatures

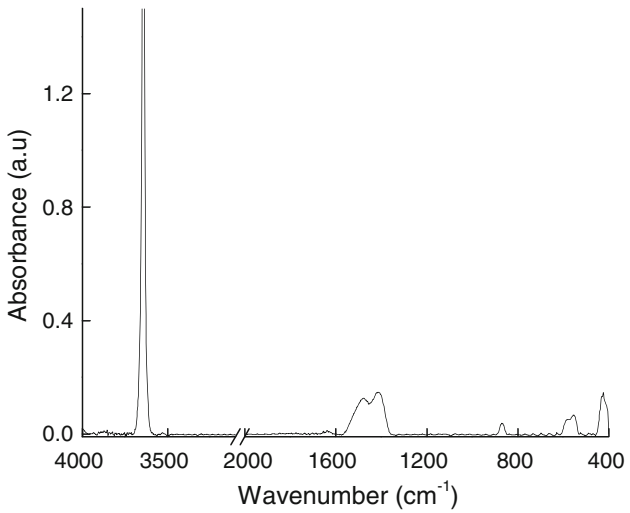


**Fig. 4** FTIR spectrum of calcium oxide (CaO) at room temperature

As the sintering temperature increased, new peaks showed up in the region of 1,100–900 $cm^{-1}$. For the samples sintered at 900–1,100°C, the FTIR patterns in this region are identical, as shown in Fig. 3c–e. Very sharp and strong peaks dominate the $v_3$ region and the band at 1,063 $cm^{-1}$ is the strongest one. At the low wave number end of the $v_3$ absorption, two weak IR peaks between 970 and 940 $cm^{-1}$ arising from $v_1$ vibration can be distinguished. The peaks in this region fit with those in the characteristics FTIR spectra of TTCP quite well [26, 35]. From the figures, the intensity ratio between the 1,063 $cm^{-1}$ band and the 3,643 $cm^{-1}$ band decreased rapidly as the sintering temperature increased, indicating more CaO formation and less TTCP in the composite. When the sintering temperature reached 1,200°C, the bands in the region of 900–1,100 $cm^{-1}$ completely vanished, implying that most TTCP disappeared from the system. The thermal decomposition behaviours of the Ti/HA composite observed in this study agree with Ning's investigation quite well [20, 22].

In Fig. 3c, d, the bands in the region of 400–650 $cm^{-1}$, corresponding to the $v_4$ and $v_2$ modes of phosphate, are identical. Apparent difference in the same region can be observed in Fig. 3b. Clear sharp peaks at 622, 505, 473,

**Table 2** Observed infrared band positions and their assignments

| Peak position ($cm^{-1}$) | Assignment | Phase | Reference |
|---|---|---|---|
| 3643 | $OH^-$ | $Ca(OH)_2$ | [34], [35], [37] |
| 3571 | $OH^-$ | HA | [27], [28], [31], [37], [39] |
| 1476, 1421 | $v_3$ ($CO_3^{2-}$) | $CaCO_3$ | [28], [35] |
| 1093, 1045, 1011, | $v_3$ ($PO_4^{3-}$) | TTCP, HA | [24], [26], [27], [31], [38] |
| 1063, 991 | $v_3$ ($PO_4^{3-}$) | TTCP | [26], [35] |
| 962 | $v_1$ ($PO_4^{3-}$) | TTCP, HA | [24], [26–28], [31], [35], [38], [39] |
| 956 | $v_1$ ($PO_4^{3-}$) | TTCP | [26], [35] |
| 870 | $v_2$ ($CO_3^{2-}$) | $CaCO_3$ | [24], [35], [37] |
| 632 | OH | HA | [27], [31], [35], [39] |
| 622, 594, 566 | $v_4$ ($PO_4^{3-}$) | TTCP | [26], [35] |
| 602, 567 | $v_4$ ($PO_4^{3-}$) | HA | [27], [31], [35], [37] |
| 505, 472, 410 | $v_2$ ($PO_4^{3-}$) | TTCP | [26], [35] |
| 472 | $v_2$ ($PO_4^{3-}$) | HA | [31], [39] |
| 427, 553 | Ca–O | CaO | [32], [33] |
| 449 | Ti–O | $CaTiO_3$ | [36] |

449, and 410 $cm^{-1}$ were detected. Peak at 622 $cm^{-1}$ is attributed to $v_4$ vibration of phosphate in TTCP and those at 505, 473, and 410 $cm^{-1}$ are the $v_2$ modes of phosphate in TTCP. The band at 449 $cm^{-1}$ comes from Ti–O vibration, which represents the $CaTiO_3$ [36]. As the sintering temperature rises, peaks in this region are getting weaker and broader. For the sample sintered at 1,100°C, the $v_4$ bands at 622 and 567 $cm^{-1}$, and $v_2$ bands at 505, 473, and 410 $cm^{-1}$, are still distinguishable (Fig. 3d). However, for the sample sintered at 1,200°C, the bands in this region are very disorderly, due to further decomposition of TTCP.

The thermal change of pure HA has been reported to occur in two stages: dehydroxylation and decomposition [37–40]. At the first stage, HA is dehydroxylated to oxyhydroxyapatite (OHA), which is a solid solution of oxyapaite (OA) and HA. With the increase in the sintering temperature, the $OH^-$ group in HA gradually decreased. A widely accepted reaction formula for the first stage is:

$$Ca_{10}(PO_4)_6(OH)_2 \rightarrow Ca_{10}(PO_4)_6O_x(OH)_{2-2x} + xH_2O$$

Due to different factors such as purity of reagents and water vapour pressure, the temperature range of dehydroxylation varies from case to case [29, 40, 41]. In this study, the FTIR spectra of the sintered samples manifested that the dehydroxylation of pure HA occurred at temperatures above 900°C. The relative intensity of the hydroxyl band decreased with the sintering temperature while that of the oxyhydroxyapatite band increased (Table 1). Up to 1,200°C, the specific peak due to the $OH^-$ stretching still exists in the spectrum, denoting that the HA has only been partially dehydroxylated and no decomposition occurred.

As the sintering temperature further increases, the decomposition of the OA, or OHA, will commence. Similar to the dehydroxylation of HA, various decomposition temperatures have been reported. Furthermore, different reaction formulas have been proposed. The most commonly accepted one is [29, 41, 42]:

$$Ca_{10}(PO_4)_6(OH)_2 \rightarrow 2Ca_3(PO_4)_2 + Ca_4O(PO_4)_2 + H_2O$$

Some investigators reported that other reaction products, such as $Ca_2P_2O_7$ and CaO, could be observed during the decomposition of HA [43]. In the study by Cihlar [41], only single calcium phosphate phase (TCP or TTCP) was discovered at a certain temperature range. The differences in the investigations were probably associated with the purity of HA and the conditions under which the decomposition was studied, especially the water vapour pressure in the atmosphere.

With the presence of Ti, the dehydroxylation of HA was completed after sintering at 900°C. Even after sintering at 800°C, decomposition of HA was noticeable (Fig. 3b). The contribution of Ti to the early completion of dehydroxylation can be explained below. At high temperatures, the valence state of Ti on the surface could be reduced through the diffusion of oxygen towards the center of the Ti particles. The dehydrated water from HA dehydroxylation reacts with the surrounding fresh Ti surface to form Ti oxides, which will further accelerate the dehydroxylation reactions. Interestingly, in the stage of decomposition, no characteristic bands of TCP or $Ca_2P_2O_7$ emerged in the FTIR spectra of the sintered samples. The predominant phases formed during sintering the Ti/HA samples were detected as TTCP and CaO. An explanation to this phenomenon is the change of Ca/P ratio in the apatite. During the thermal process, diffusion of calcium and phosphorous ions into the Ti substrate has been detected in previous

studies [44–46]. On the basis of its smaller radii and lower activation energy, the phosphorous ions could diffuse more rapidly into the Ti substrate to form Ti phosphate, which induces a higher Ca/P ratio in the apatite. As shown in the equilibrium phase diagram, when Ca/P ratio is higher than 1.67, TTCP and CaO will be the main phase of decomposed HA at room temperature [44, 47]. Another possible reason is the reaction between TCP and CaO occurred during the process as:

$$Ca_3(PO_4)_2 + CaO \rightarrow Ca_4O(PO_4)_2$$

at a certain temperature range, which has been confirmed in pure HA decomposition [48]. Therefore, with the presence of Ti, the main thermal decomposition phases of HA are CaO and TTCP. As the temperature increases, TTCP will finally decompose to form CaO, which may also be attributed to the deficit of phosphorus caused by diffusion.

## 4 Conclusions

The phase change of HA in the Ti/HA biocomposite sintered under various conditions was characterized by FTIR. The results showed that the decomposition of HA goes through two stages: dehydroxylation and decomposition. Pure HA alone was stable in argon atmosphere and no decomposition occurred at temperatures up to 1,200°C. Quantitative study of the ratios of band intensities, however, demonstrated that dehydroxylation of HA did occur during sintering, and is promoted by increasing the sintering temperature. The presence of Ti accelerated the dehydroxylation of HA, probably through the reaction of the fresh Ti surface with the dehydrated water. In Ti/HA composite, decomposition of HA can be identified at a temperature as low as 800°C. TTCP and CaO were the most prominent products of the decomposition reactions, and $CaTiO_3$ was also detected in the system. The study exemplified the capability of FTIR as an effective technique to characterize the phase change of a biocomposite during the thermal process.

**Acknowledgments** This work is supported by the Natural Science and Engineering Research Council of Canada. The valuable discussions and help from Prof. P.J Ragogna, Mr. Jason L. Dutton and Mr. Caleb Martin of the University of Western Ontario related to this research work are gratefully acknowledged.

## References

1. L. Hong, H.C. Xu, K. de Groot, J. Biomed. Mater. Res. **26**, 7 (1992). doi:10.1002/jbm.820260103
2. J.T. Edwards, J.B. Brunski, H.W. Higuchi, J. Biomed. Mater. Res. **36**, 454 (1997). doi:10.1002/(SICI)1097-4636(19970915)36:4<454::AID-JBM3>3.0.CO;2-D
3. U. Ripamonti, J. Bone Joint Surg. **73A**, 692 (1991)
4. J.H. Kuhne, R. Bartle, B. Frisch, Acta Orthop. Scand. **65**(3), 246 (1994)
5. J.C. Elliot, P.E. Machie, R.A. Yong, Science **180**, 1055 (1973). doi:10.1126/science.180.4090.1055
6. L.L. Hench, J. Am. Ceram. Soc. **81**, 1705 (1998)
7. H. Aoki, *Science and Medical Applications of Hydroxyapatite* (Takayama, Tokyo, 1991), p. 137
8. K.S. Vecchio, X. Zhang, J.B. Massie, M. Wang, C.W. Kim, Acta Biomater. **3**, 910 (2007). doi:10.1016/j.actbio.2007.06.003
9. G. de With, H.J.A. Candijk, N. Hattu, K. Prijs, J. Mater. Sci. **16**, 1592 (1981). doi:10.1007/BF02396876
10. O. Prokopiev, I. Sevostianov, Mater. Sci. Eng. A **431**, 218 (2006). doi:10.1016/j.msea.2006.05.158
11. Y.C. Fung, *Biomechanics: Mechanical Properties of Living tissues* (Springer-Verlag, New York, 1993), p. 510
12. R.V. Noort, J. Mater. Sci. **22**, 3801 (1987). doi:10.1007/BF01133326
13. M. Long, H.J. Rack, Biomaterials **19**, 1621 (1998). doi:10.1016/S0142-9612(97)00146-4
14. A. Biship, C.Y. Lin, M. Navaratnam, R.D. Rawlings, H.B. Mcshane, J. Mater. Sci. Lett. **12**, 1516 (1993)
15. C.L. Chu, J.C. Zhu, Z.D. Yin, S.D. Wang, Mater. Sci. Eng. A **271**, 95 (1999). doi:10.1016/S0921-5093(99)00152-5
16. C.L. Chu, J.C. Zhu, Z.D. Yin, P.H. Lin, Mater. Sci. Eng. A **316**, 205 (2001). doi:10.1016/S0921-5093(01)01239-4
17. C.L. Chu, J.C. Zhu, Z.D. Yin, P.H. Lin, Mater. Sci. Eng. A **348**, 244 (2003). doi:10.1016/S0921-5093(02)00738-4
18. C.Q. Ning, Y. Zhou, H.L. Wang, D.C. Jia, T.C. Lei, J. Mater. Sci. Lett. **19**, 1243 (2000). doi:10.1023/A:1006725529837
19. C.L. Chu, X.Y. Xue, J.C. Zhu, Z.D. Yin, J. Mater. Sci. Mater. Med. **17**, 245 (2006). doi:10.1007/s10856-006-7310-6
20. C.Q. Ning, Y. Zhou, Biomaterials **23**, 2909 (2002). doi:10.1016/S0142-9612(01)00419-7
21. J. Weng, X.G. Liu, X.D. Zhang, X.Y. Ji, J. Mater. Sci. Lett. **13**, 159 (1994). doi:10.1007/BF00278148
22. C.Q. Ning, Y. Zhou, Biomaterials **25**, 3379 (2004). doi:10.1016/j.biomaterials.2003.10.017
23. C. Popa, V. Simon, I. Vida-Simiti, G. Batin, V. Candea, S. Simon, J. Mater. Sci. Mater. Med. **16**, 1165 (2005). doi:10.1007/s10856-005-4724-5
24. A. Antonakos, E. Largokapis, T. Leventouri, Biomaterials **28**, 3043 (2007). doi:10.1016/j.biomaterials.2007.02.028
25. A. Jillavenkatesa, R.A. Condrate Sr, Spectrosc. Lett. **31**, 1619 (1998). doi:10.1080/00387019808007439
26. U. Posset, E. Locklin, R. Thull, W. Kiefer, J. Biomed. Mater. Res. **40**, 640 (1998). doi:10.1002/(SICI)1097-4636(19980615)40:4<640::AID-JBM16>3.0.CO;2-J
27. A. Rapacz-kmita, C. Paluszkiewicz, A. Slosarczyk, Z. Paszkiewicz, J. Mol. Struct. **744–47**, 653 (2005). doi:10.1016/j.molstruc.2004.11.070
28. H. Nishikawa, Mater. Lett. **50**, 364 (2001). doi:10.1016/S0167-577X(01)00318-4
29. K.A. Gross, C.C. Berndt, P. Stephens, R. Dinnebier, J. Mater. Sci. **33**, 3985 (1998). doi:10.1023/A:1004605014652
30. D.M. Liu, H.M. Chou, J.D. Wu, J. Mater. Sci. Mater. Med. **5**, 147 (1994). doi:10.1007/BF00053335
31. I. Rehman, W. Bonfield, J. Mater. Sci. Mater. Med. **8**, 1 (1997). doi:10.1023/A:1018570213546
32. M. Kukura, L.C. Bell, A.M. Posner, J.P. Quirk, J. Phys. Chem. **76**, 900 (1972). doi:10.1021/j100650a019
33. R.A. Nyquist, R.O. Rageli, *Handbook of Infrared and Raman Spectra of Inorganic Compounds and Organic Salts. Vol.4: Infrared Spectra of Inorganic Compounds (3800–45 cm⁻1)* (Academic, San Diego, 1997), p. 207

34. G. Penel, G. Leroy, C. Rey, B. Sombert, J.P. Huvenne, E. Bres, J. Mater. Sci. **8**, 271 (1997). doi:10.1023/A:1018504126866
35. Y. Sargin, M. Kizilyalli, C. Telli, H. Guler, J. Eur. Ceram. Soc. **17**, 963 (1997). doi:10.1016/S0955-2219(96)00196-3
36. M.K. Gergs, H.A. Said, M. Donogol, H.A. Aly, Int. J. Mater. Sci. **2**, 81 (2007)
37. S. Jalota, A.C. Tas, S.B. Bhaduri, J. Am. Ceram. Soc. **88**, 3353 (2005). doi:10.1111/j.1551-2916.2005.00623.x
38. C.C. Ribeiro, I. Gibson, M.A. Barbosa, Biomaterials **27**, 1749 (2006). doi:10.1016/j.biomaterials.2005.09.043
39. B.O. Fowler, Inorg. Chem. **13**, 194 (1974). doi:10.1021/ic50131a039
40. T. Wang, A. Dorner-Reisel, Mater. Lett. **58**, 3025 (2004). doi:10.1016/j.matlet.2004.05.033
41. J. Cihlar, A. Buchal, M. Trunec, J. Mater. Sci. **34**, 6121 (1999). doi:10.1023/A:1004769820545
42. C. Liao, F. Lin, K. Chen, J. Sun, Biomaterials **20**, 1807 (1999). doi:10.1016/S0142-9612(99)00076-9
43. J. Zhou, X. Zhang, J. Chen, S. Zeng, K. de Groot, J. Mater. Sci. Mater. Med. **4**, 83 (1993). doi:10.1007/BF00122983
44. K.A. Gross, C.C. Berndt, J. Biomed. Mater. Res. **39**, 580 (1998). doi:10.1002/(SICI)1097-4636(19980315)39:4<580::AID-JBM12>3.0.CO;2-B
45. M.J. Filiaggi, R.M. Pilliar, N.A. Coombs, J. Biomed. Mater. Res. **27**, 191 (1993). doi:10.1002/jbm.820270208
46. H. Ji, P.M. Marquis, Biomaterials **14**, 64 (1993). doi:10.1016/0142-9612(93)90077-F
47. E.R. Kreidler, F.A. Hummel, Inorg. Chem. **6**, 884 (1967). doi:10.1021/ic50051a007
48. J. Chen, W. Tong, C. Yang, J. Feng, X. Zhang, J. Biomed. Mater. Res. **34**, 15 (1997). doi:10.1002/(SICI)1097-4636(199701)34:1<15::AID-JBM3>3.0.CO;2-Q